Chemically non-equilibrium model of decaying N2 arcs in a model circuit breaker

メタデータ	言語: English 出版者: 公開日: 2017-10-03 キーワード (Ja): キーワード (En): 作成者: Sun, Hao, Tanaka, Yasunori, Rong, Mingzhe, Uesugi, Yoshihiko, Ishijima, Tatsuo メールアドレス: 所属:
URL	http://hdl.handle.net/2297/45477

Chemically non-equilibrium model of decaying N_2 arcs in a model circuit breaker

Hao Sun[1], Yasunori Tanaka[2,3], Mingzhe Rong[1], Yoshihiko Uesugi[2,3], Tatsuo Ishijima[2,3]

1-State Key Laboratory of Electrical Insulation and Power Equipment, Xi'an Jiaotong University, Xi'an Shaanxi 710049, People's Republic of China
2-Faculty of Electrical and Computer Engineering, Kanazawa University, Kakuma, Kanazawa 920-1192 Japan
3-Research Center for Sustainable Energy, Kanazawa University, Kakuma, Kanazawa 920-1192 Japan

***Abstract*—Nitrogen gas has been investigated as one of the candidate substitutes for SF_6 in a high-voltage circuit breaker (HVCB) and also in a low-voltage interrupter. In this paper, a chemically non-equilibrium model was established to investigate N_2 arc plasmas in the decaying phase during current interruption in a model circuit breaker. Unlike the conventional model assuming local thermodynamic equilibrium, i.e. both chemical equilibrium and thermal equilibrium, in this work a chemically non-equilibrium model was developed for N_2 arc plasmas. Thermal non-equilibrium effects were neglected, meaning a one-temperature model was adopted. The developed model took into account 5 species such as N_2, N, N_2^+, N^+ and e^-, and 22 chemical reactions including electron impact ionizations, heavy particles impact dissociations and their backward reactions. Temperature dependent reaction rates were used for all considered reactions. The species composition in N_2 arc plasma was calculated by solving the mass conservation equation of each species considering diffusion, convection and reaction effects. Then the influence of the chemically non-equilibrium composition on the arc behavior was calculated by updating the thermodynamic and transport properties at each iterative step. Finally, for the decaying N_2 arc plasma under a free recovery phase, the time evolutions were derived in the profiles of the temperature and the number densities for each species. The results in this work were compared with the calculated results based on the chemical equilibrium assumption.**

Keywords—non-chemically equilibrium model; local thermodynamic equilibrium model; decaying N_2 arcs; mass conservation equation of each species; chemical reactions; thermodynamic and transport properties

I. INTRODUCTION

Sulfur hexafluoride (SF_6) gas is used almost exclusively in high-voltage circuit-breakers because of its high insulation strength and its high fault-current interruption capability. However, SF_6 has an extremely-high global warming potential (GWP), 22900 times greater than that of CO_2 per unit mass , and is regulated as a greenhouse gas following the 3rd Conference of the Parties to the United Nation Framework Convention on Climate Change (COP3) [1,2].

Therefore, in recent years there have been intense efforts to find an environmentally-friendly gas to replace SF_6. N_2 has been investigated as one of the substitutes by many researchers. In Christophorou et al.'s book, N_2, as one of the possible alternative gases of SF_6 for possible immediate or future use in existing or modified electrical equipment, was discussed [3]. Gleizes et al. calculated the thermodynamic properties, transport coefficients and net emission coefficient in SF_6-N_2, which provided the fundamental data to calculate the arc plasma [4-5]. Pinheiro and Loureiro investigated the effective ionization coefficients and electron drift velocities in gas mixture of SF_6 with N_2 from Boltzmann analysis, which give us a better understanding of the electrical breakdown in this gas [6].

There are two crucial phases for the arc interruption in the circuit breaker [7]. One is the arc ignition after the two electrodes are separated. The magneto-hydro-dynamics (MHD) method [8-9] is quite common for the calculation of the arc plasma and the local thermodynamic equilibrium (LTE) model, which assumes the temperatures of the heavy particles and the electrons are identical and all the chemical reactions reach the equilibrium, is introduced in MHD for the simulation of the arc ignition. However, in the phase of the post arc after current zero, the electron density decays fast and the non-chemical equilibrium (non-CE) occurs due to the lower chemical reaction rate at the decaying temperature, and thus the departure from LTE takes place. The two-temperature (2T) model has been adopted in the decaying arc [10] while a self-consistent non-CE model was not yet used accounting for reaction heat as well as thermodynamic and transport properties except for Tanaka et al.'s work [11-12].

In this paper, an axis-symmetric MHD model was developed for the N_2 decaying arc after current zero considering the non-CE. The developed model took into account 5 species such as N_2, N, N_2^+, N^+ and e^-, and 22 chemical reactions including electron impact ionizations, heavy particles impact dissociations and their backward reactions. Temperature dependent reaction rates were used for all considered reactions. The species composition in N_2 arc plasma was calculated by solving the mass conservation equation of each species considering diffusion, convection and reaction effects. Then, the influence of the non-CE composition on the arc behavior was calculated by updating the thermodynamic and transport properties at each iterative step. Finally, for the decaying N_2 arc plasma after a current from 50 to 0 A under a free recovery phase, the time evolutions were derived in the profiles of the temperature and the number densities for each

species. The results in this work were also compared with the calculated results based on the chemical equilibrium assumption.

II. MODELLING OF THE NON-CE ARCS

A. Hypothesis

The non-CE model in this calculation was established based on the following assumptions: (i) Thermal non-equilibrium effects were neglected, meaning a one-temperature model was adopted. (ii) The arc plasma was axis-symmetric. (iii) The k-ε turbulence model was adopted. (iv) The optically thin assumption was established. (v) The collision cross sections between the particles assumed that the particles were spheres with a constant radius and the collision integrals were obtained by summing the cross sections of the two species for simplicity.

B. Governing equations

There are three most crucial aspects that should be considered in the non-CE model: (i) The non-CE species compositions must be obtained at each iteration based on the chemical reaction kinetics. (ii) Then the thermodynamic and transport properties should be derived from the non-equilibrium species compositions and adopted at each iteration. (iii) The influence of the non-CE condition on the energy should also be taken into account.

Therefore, based on all the hypothesis mentioned above, this calculation should be governed by the following equations:

Mass transport equation of each of species j

$$\frac{\partial \rho Y_j}{\partial t} + \nabla \cdot \left(\vec{u}\rho Y_j\right) = \nabla \cdot \left(\rho D_j \nabla Y_j\right) + S_j \tag{1}$$

$$S_j = m_j \sum_l^L \left(\beta_{jl}^r - \beta_{jl}^f\right)\left(k_l^f \prod_{i=1}^N n_i^{\beta_{il}^f} - k_l^r \prod_{i=1}^N n_i^{\beta_{il}^r}\right) \tag{2}$$

$$D_j = \frac{1 - Y_j}{\sum_{k \neq j}\left(x_k / D_{jk}\right)} \tag{3}$$

$$D_{jk} = \frac{\kappa T}{p}\frac{1}{\Delta_{kj}^{(1)}} \tag{4}$$

$$\frac{1}{\Delta_{kj}^{(1)}} = \frac{3}{8}\left[\frac{\pi\kappa T\left(m_i + m_j\right)}{2 m_i m_j}\right]^{1/2}\frac{1}{\pi\Omega_{ij}} \tag{5}$$

The ideal gas equation

$$p = \sum_j n_j \kappa T \tag{6}$$

Relation between the number density and mass fraction

$$n_j = \frac{\rho Y_j}{m_j} \tag{7}$$

$$\rho = \sum_j n_j m_j \tag{8}$$

Equation (1)-(8) describes the derivation of the non-CE species compositions from the chemical reaction kinetics, where ρ is the gas density, Y_j is the mass fraction of species j, $\boldsymbol{u}$ is the gas flow velocity vector, m_j is the mass of the species j, β_{jl} is the stoichiometric coefficient of species j for reaction l, k_l^f and k_l^r is the rate coefficient in reaction l for forward reaction and reverse reaction, respectively, x_k is the mole fraction of species k, T is the temperature, p is the pressure, κ is the Boltzmann constant, Ω_{ij} is the collision integrals between species i and j mentioned in the previous section and n_j is the number density of species j.

The MHD calculation also requires the thermodynamic and transport properties of the hot gas, including gas density ρ, thermal conductivity k, and viscosity η. Different from LTE model, in which all the properties are calculated in advances and obtained by interpolation as a function of temperature and pressure during the calculation, in the non-CE model these properties should be self-consistently calculated based on the non-equilibrium compositions and updated at each iteration. The calculation of the transport properties was based on the first-order approximation of the Chapman–Enskog method [12] in the following equations.

$$k = \frac{15}{4}\kappa \sum_j \frac{n_j}{\sum_j \xi_{ij} n_i \Delta_{ij}^{(2)}} \tag{9}$$

$$\xi_{ij} = 1 + \frac{\left(1 - m_i / m_j\right)\left(0.45 - 2.54 m_i / m_j\right)}{\left(1 + m_i / m_j\right)^2} \tag{10}$$

$$\eta = \sum_{j=1}^N \frac{m_j n_j}{\sum_{i=1}^N n_i \Delta_{ij}^{(2)}} \tag{11}$$

$$\frac{1}{\Delta_{ij}^{(2)}} = \frac{5}{16}\left[\frac{\pi\kappa T\left(m_i + m_j\right)}{2 m_i m_j}\right]^{1/2}\frac{1}{\pi\Omega_{ij}} \tag{12}$$

For the fluid calculation, the basic mass equation, momentum equation are the same as those in the LTE model. However, there should be some modification on the energy equation to include the non-CE effect.

Mass conservation equation

$$\frac{\partial \rho}{\partial t} + \nabla \cdot \left(\vec{u}\rho\right) = 0 \tag{13}$$

Momentum conservation equation

$$\frac{\partial}{\partial t}\left(\rho\vec{u}\right) + \nabla \cdot \left(\rho\vec{u}\vec{u}\right) = -\nabla p + \nabla \cdot \left(\vec{\tau}\right) \tag{14}$$

Energy equations

$$\begin{aligned}&\frac{\partial}{\partial t}\left(\rho E\right) + \nabla \cdot \left(\vec{v}\left(\rho E + p\right)\right) = \\ &\nabla \cdot \left(k_{eff}\nabla T + \left(\overrightarrow{\tau_{eff}} \cdot \vec{v}\right) + \sum_j^N \rho D_j h_j \nabla Y_j\right) - P_{rad}\end{aligned} \tag{15}$$

$$E = h - \frac{p}{\rho} + \frac{u^2}{2} \tag{16}$$

$$h=\sum_j \frac{Y_j}{m_j}\left(\frac{5}{2}\kappa T+\kappa T^2\frac{\partial \ln Z_j}{\partial T}+\Delta H_{fj}\right) \tag{17}$$

$$P_{rad}=4\pi\varepsilon \tag{18}$$

In (14) τ is the stress tensor. The k_{eff} and τ_{eff} in the energy equation are the effective thermal conductivity and stress tensor considering the turbulence effect. Z_j is the partition function of species j, ε is the net emission coefficient and ΔH_{fj} is the standard enthalpy of formation of species j. It can be noted that in the energy equation the specific heat was excluded in this calculation because (17) gives the relation between enthalpy and temperature directly and the specific heat was considered implicitly. It should be noted that the third term of the diffusion in (15) represents the energy transportation due to the species diffusion, which was neglected in the LTE model. Moreover, the last term in (17) is the standard enthalpy of formation and by adding this term the non-CE effect on the chemical reaction energy can be calculated implicitly in the energy equation. Since this non-CE model deals with the arc plasma after the current drops to zero, the Joule heat was not included in the energy equation.

C. *Selection of the species and reactions*

It is important to determine how many species should be included in this calculation. In fact in the hot N_2, there are several dissociation and ionization products, such as N, N_2^+, N^+, N^{2+} and N^{3+}. However, since the steady current in this calculation is 50 A and the highest temperature at the steady state is about 14000 K, in this case only N_2, N, N_2^+, N^+ and e^- were taken into account.

In present calculation 11 reactions were considered. All the reactions are listed as follows:

$$N_2+N_2 \rightarrow N+N+N_2 \tag{19}$$

$$N_2+N \rightarrow N+N+N \tag{20}$$

$$N_2+e \rightarrow N+N+e \tag{21}$$

$$N+e \rightarrow N^++e+e \tag{22}$$

$$N_2^++N_2+e \rightarrow N_2+N_2 \tag{23}$$

$$N_2^++N+e \rightarrow N+N_2 \tag{24}$$

$$N^++N_2+e \rightarrow N+N_2 \tag{25}$$

$$N^++N+e \rightarrow N+N \tag{26}$$

$$N_2+e \rightarrow N_2^++e+e \tag{27}$$

$$N+N \rightarrow N_2^++e\,. \tag{28}$$

$$N_2^++N \rightarrow N^++N_2 \tag{29}$$

TABLE I. THE THREE COEFFICIENTS OF ALL THE REACTIONS

Number	a_{1l}	a_{2l}	a_{3l}	*Reaction heat*
19	1.17×10^{-8}	-1.6	113260	9.759
20	5.0×10^{-8}	-1.6	113260	9.759
21	5.0×10^{-6}	-1.6	113260	9.759
22	4.17×10^{3}	0	168200	14.534
23	6.07×10^{-34}	-2.5	0	-15.580
24	1.66×10^{-35}	-2.5	0	-15.580
25	6.07×10^{-34}	-2.5	0	-14.534
26	1.66×10^{-35}	-2.5	0	-14.534
27	1.88×10^{-18}	0.85	179000	15.580
28	3.33×10^{-17}	0	67500	5.821
29	1.30×10^{-19}	0.5	0	-1.047

The forward reaction rates in all the above reactions can be obtained from (30):

$$k_l^f=a_{1l}T^{a_{2l}}\exp\left(-\frac{a_{3l}}{T}\right). \tag{30}$$

The three coefficients in (30) are from the previous literature [11], as listed in TABLE I.

The reverse reaction rates were evaluated according to the principle of detailed balancing [11]. Taking the reaction (19) as an example, the reverse reaction rate in reaction (19) is as follows:

$$k_1^r=k_1^f\left(\frac{h_p^2 m_{N_2}}{2\pi m_N m_N \kappa T}\right)^{3/2}\frac{Z_{N_2}}{Z_N^2}\exp\left(\frac{\psi_{reac1}}{\kappa T}\right). \tag{31}$$

In (31) h_p is the Planck constant and ψ_{reac1} is the reaction heat of this reaction, which is also obtained from the previous literature [11].

D. *Calcualtion model, boundary conditions and initial value*

Fig.1 shows the calculation domain of a model circuit breaker in present calculation. As it is mentioned above, this model is axis-symmetric so that Fig.1 shows half of the cross section and r = 0 mm represents the axis of the device. As it can be seen, the gas flows in at a velocity of 1.768 m/s from the left entrance and flows out on the right side. Out of the nozzle the pressure was set as 101325 Pa while the temperature was set as 300 K.

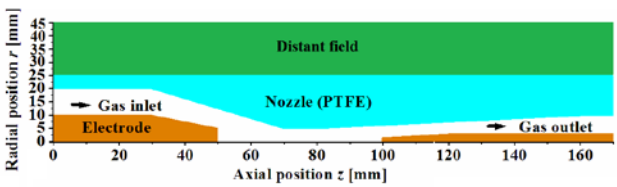

Fig.1 Calculation domain

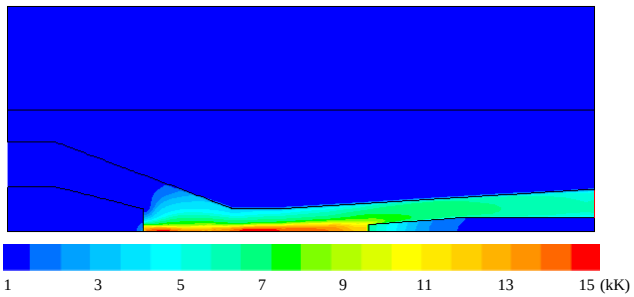

Fig.2 The temperature profiles for the post arc calculation at t=0 as the initial value

For the steady-state arc, the left electrode was the anode and the current was 50 A DC in this calculation. The green area on the upside was established as the distant field for the electromagnetic calculation of the steady-state arc. In the steady-state calculation the LTE model was adopted and the electromagnetic field was solved using the following equations.

$$\vec{j} = \sigma \vec{E} = -\sigma \nabla \varphi = -\sigma \left(\frac{\partial \varphi}{\partial r} \vec{e}_r + \frac{\partial \varphi}{\partial z} \vec{e}_z \right) \tag{32}$$

$$\nabla \cdot \vec{j} = 0 \tag{33}$$

$$\nabla^2 A_r = \mu_0 j_r - \frac{A_r}{r^2} \tag{34}$$

$$\nabla^2 A_z = \mu_0 j_z \tag{35}$$

where $\vec{j}$ is the current density, $\vec{E}$ is the electrical field, φ is the electrical potential, σ is the electrical conductivity, μ_0 is the relative permeability in the vacuum, and A_r and A_z is the component of the magnetic vector potential of the radial and axial direction, respectively. The influence of the Lorentz force on the momentum equation as well as the Joule heat on energy equation was considered respectively.

The initial value of the arc plasma after current zero in this calculation, which is temperature profile, pressure profile, velocity profile, species composition profiles and so on, was obtained from the results of the steady-state calculation mentioned above. Fig.2 shows the temperature profile for the post arc calculation at t=0. It can be noted that at the axis the highest temperature of the arc plasma was around 14000 K. At t=0, the current drops from 50 A to 0 A, which means the electromagnetic field was not calculated in present work.

III. RESULTS AND DISCUSSION

A. *Transient temperature profiles*

Fig. 3 shows the transient temperature profiles between the two electrodes from t=0 to t=100 μs in the non-CE model. It can be clearly inspected that at the first 20 μs the highest temperature decreases sharply from around 14000 K to 8000 K. The reason is that in this temperature range the radiation coefficient in (18) is quite high and the temperature decay is dominant by the radiation. From t=50 μs the temperature decays slowly mainly due to the convection and diffusion as in (15). And it should also be noted that although the temperature

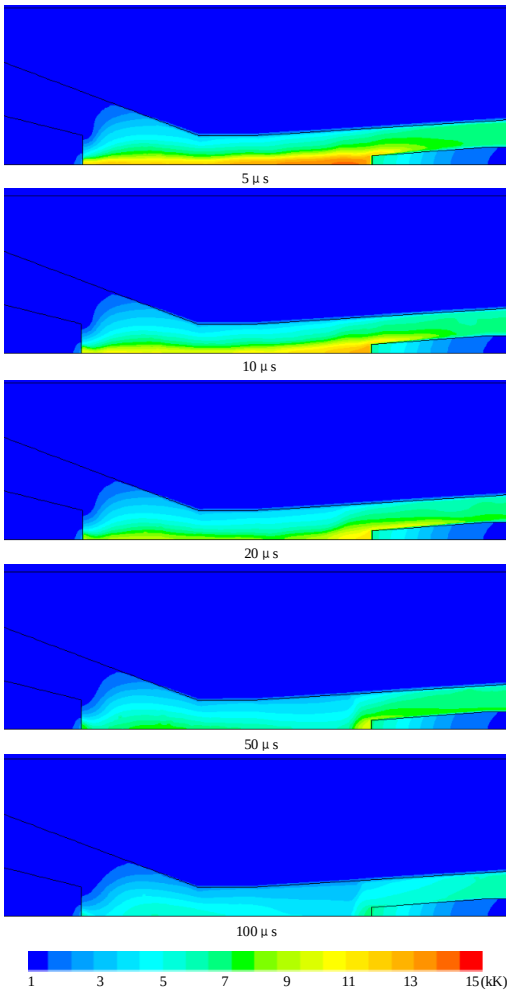

Fig.3 The time evolution of temperature profiles by non-CE model

decays rapidly at z=80 mm, which is at the nozzle throat inlet as it is shown in Fig.1, the temperature decays slowly at z=100 mm, which is at the position near the cathode. The reason will be discussed in the next section in detail. Finally, the temperature drops to around 4000 K at t=100 μs.

The results by the non-CE model were also compared with those by the LTE model for a better understanding of the difference between these two models. To ensure the consistency in the two models, in LTE model only the equilibrium compositions were obtained by interpolation and the transport properties were derived by (9)-(12) based on the first-order approximation of the Chapman–Enskog method, which were the same as those in the non-CE model mentioned above. It should be noted that since in the LTE model (1)-(8) was not solved during the calculation, in (15) the third term of the diffusion was not included. Fig.4 shows the transient temperature profiles between the two electrodes from t=0 to t=100 μs in the LTE model.

Figs.3 and 4 illustrate that before t=5 μs the temperature profiles have a week dependence on the kind of the models. The reason is that before t=5 μs the temperature is still quite high and thus within this short time the non-CE effect is not obvious yet. From t=10 μs to t=50 μs, there are two main differences between the two models.One is that the temperature

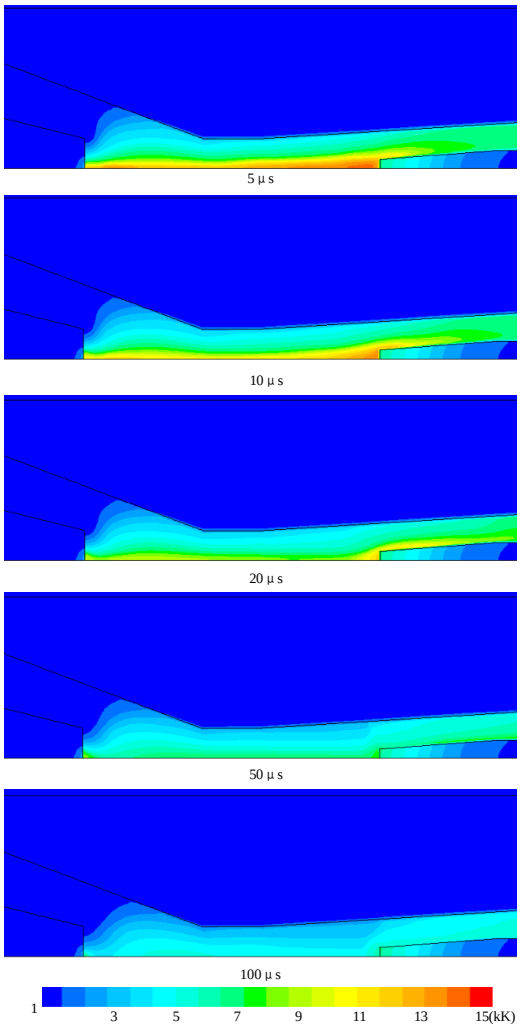

Fig.4 The time evolution of temperature profiles by LTE model

temperature by the non-CE at the nozzle throat inlet decays more rapidly than the LTE model. On the contrary, it must be noted that the temperature in the non-CE near the cathode (z=100 mm) decays more slowly. The reason for this phenomenon will be further discussed in the next section.

B. Temperature variations both at the nozzle throat inlet and near the cathode.

The time evolutions of temperature in both non-CE model and LTE model at the nozzle throat inlet is shown in Fig.5 for easier inspection, as well as those near the electrodes in Fig.6.

Fig.5 clearly illustrates that the temperature at the nozzle throat decreases faster in the non-CE model than that in LTE model, especially at t=20-100 μs, and the largest temperature difference can be around 1000 K between the two models at the same moment. During the temperature decay, the ions N^+ and N_2^+ tends to be recombined with the electrons and the N tends to be associated to N_2. As Table I shows, all these recombination and association reactions are exothermic. However, due to the finite delay of these reactions in the non-CE model, there is less reaction heat released into the arc area so that the temperature decreases more rapidly.

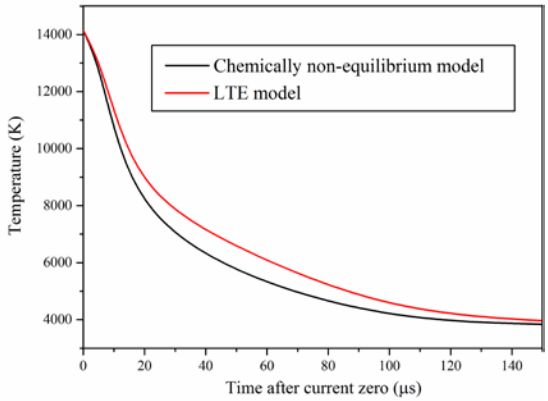

Fig.5 The time evolution of temperature at the nozzle throat (z=80 mm)

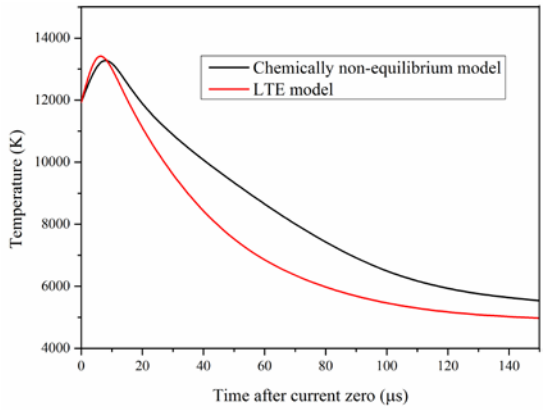

Fig.6 The time evolution of temperature near the cathode (z=100 mm)

Fig.6 presents the temperature variation near the cathode. During the first 10 μs after current zero there is an increase in the temperature from 11000 K to 13500 K in both the two models. Judging from the contours in Fig.3-4, the reason is that the high temperature area at the upstream of the gas flow is transported to the area close to the cathode, mainly caused by the convection in (15) since the gas flow in the high temperature area is quite strong. After t=10 μs the temperature in non-CE decreases more slowly than that in LTE model. Eq. (1) illustrates that the non-CE model includes the transportation of the species due to convection and diffusion, which is neglected in the LTE model. Therefore, the transportation of the species from the upstream to the cathode accelerates the recombination and association in this area and more reaction heat is released.

C. Composition Variation

Fig.7 presents the time evolution of species compositions at the nozzle throat. Since the electrons are mainly ionized from the N and its number density approximates the N^+'s, the number density of electrons is not included in this figure for easier inspection. It clearly indicates that the time evolution of species compositions in the non-CE model lags behind that in the LTE model, the difference between the two models increases with the time, especially in the N^+ and N_2^+ after t=50 μs. There are two main reasons: the temperature decay with the time leads to the decrease in the reaction rate, as (30) indicates, which makes the all the reactions more difficult to reach equilibrium; the reaction rates of the reactions involving e^-, N^+

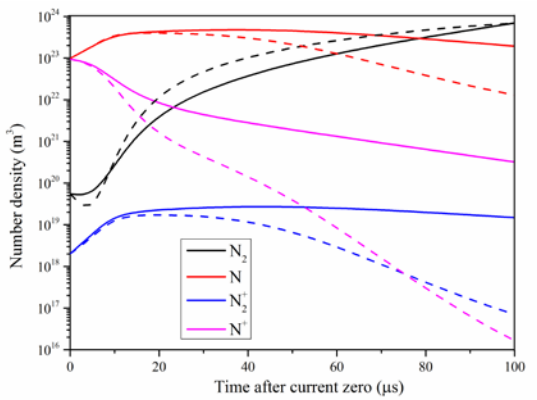

Fig.7 Time evolution of species compositions at the nozzle throat (z=80 mm)

(The solid line: by non-CE; the dash line: by LTE)

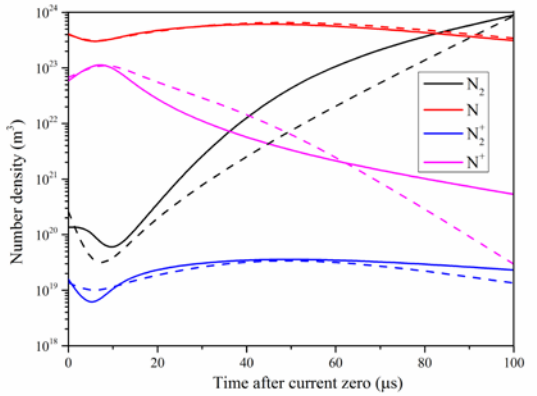

Fig.8 The time evolution of species compositions near the cathode (z=100 mm)

(The solid line: by non-CE; the dash line: by LTE)

and N_2^+ will be much lower since the number densities of the three species are quite low.

Fig.8 presents the time evolution of species compositions near the cathode. The general trend of the time-varying species compositions is opposite to that at the throat inlet. The number density changes of N_2, N and N^+ in the non-CE model are prior to those in LTE model. This probably arises from the transportation of the particles from the upstream to the cathode due to the convection and diffusion as it is shown in (1). This transportation will force the number density of N_2 to higher value and the number densities of N^+ and N to lower value near the cathodes in this area, respectively. It should also be noted that inversely the number density of N^+ decreases more slowly after t=60 μs in the non-CE model again. The reason is that as the temperature decay, most of the electrons and N^+ will recombine into N in the whole area and the non-CE effect becomes dominant again compared to the influence by the particle transportation. As to the N_2^+, since the temperature is at the range from 5000 K to 14000 K near the cathode in this case, the number density of N_2^+ is quite low and thus the non-CE effect is always dominant.

IV. CONCLUSIONS

In this work a chemically non-equilibrium model was developed for N_2 arc plasmas. Thermal non-equilibrium effects were neglected, meaning a one-temperature model was adopted. The developed model took into account 5 species such as N_2, N, N_2^+, N^+ and e^-, and 22 chemical reactions including electron impact ionizations, heavy particles impact dissociations and their backward reactions. Temperature dependent reaction rates were used for all considered reactions. The species composition in N_2 arc plasma was calculated by solving the mass conservation equation of each species considering diffusion, convection and reaction effects. Then the influence of the chemically non-equilibrium composition on the arc behavior was calculated by updating the thermodynamic and transport properties at each iterative step. Finally, for the decaying N_2 arc plasma under a free recovery phase, the time evolutions were derived in the profiles of the temperature and the number densities for each species.

The results indicate that compared with the calculation by the LTE model, the temperature at the nozzle throat decreases faster in the non-CE model due to the delay of recombination and association exothermic reactions. On the contrary, the temperature in non-CE decreases more slowly. This arises from the transportation of the species due to convection and diffusion, which is neglected in the LTE model. The present calculation should be further validated by the experimental results in the future work.

ACKNOWLEDGMENT

This work was supported in part by ……..National Key Basic Research Program of China (973 Program) (2015CB251002)

REFERENCES

[1] L. Christophorou, J. Olthoff, and R. Van Brunt, IEEE Electr. Insul. Mag. 13, 20 (1997).

[2] J. L. Hernandez-Avila, E. Basurto, and J. de Urquijo, J. Phys. D: Appl. Phys. 35, 2264 (2002)..

[3] Loucas G. Christophorou; James K. Olthoff; David S. Green; NIST TN-1425, 48 pp, November 01, 1997.

[4] A Gleizes, B Rahmani, J J Gonzalez and B Liani, 1991 J. Phys. D: Appl. Phys. 24 1300

[5] A. Gleizes, M. Razafinimanana, S. Vacquie, Plasma Chemistry and Plasma Processing, March 1986, Volume 6, Issue 1, pp 65-78

[6] M J Pinheiro and J Loureiro, 2002 J. Phys. D: Appl. Phys. 35 3077

[7] H Sun, M Rong, Z Chen, C Hou, Y Sun, Plasma Science, IEEE Transactions on (Volume:42 , Issue: 10) Page(s):2706 – 2707, 2014.

[8] Ma Ruiguang, Rong Mingzhe, Yang Fei, Wu Yi, Sun Hao, Yuan Duanlei, Wang Haiyan, Niu Chunping, IEEE Transactions on Plasma Science, Volume:41, Issue: 9 Page:2551 – 2560,Sep. 2013.

[9] Y. Wu, M. Rong, Z. Q. Sun, X. Wang, F. Yang, and X. Li, J. Phys. D, Appl. Phys. , vol. 40, no. 3, pp. 795–802, Jan. 2007.

[10] W. Z. Wang, J. D. Yan, M. Z. Rong, A. B. Murphy, and J. W. Spencer, J. Phys. D: Appl. Phys 46, 065203 (2013).

[11] Y. Tanaka, T Michishita and Y Uesugi, Plasma Sources Sci. Technol. 14 (2005) 134–151

[12] Y Tanaka and K Suzuki, IEEE Transaction on Power Delivery, VOL. 28, NO.4, OCTOBER 2013